Near Earth Asteroid Rendezvous: Mission Summary

Andrew F. Cheng
The Johns Hopkins Applied Physics Laboratory

On February 14, 2000, the Near Earth Asteroid Rendezvous spacecraft (*NEAR Shoemaker*) began the first orbital study of an asteroid, the near-Earth object 433 Eros. Almost a year later, on February 12, 2001, *NEAR Shoemaker* completed its mission by landing on the asteroid and acquiring data from its surface. *NEAR Shoemaker*'s intensive study has found an average density of 2.67 ± 0.03, almost uniform within the asteroid. Based upon solar fluorescence X-ray spectra obtained from orbit, the abundance of major rock-forming elements at Eros may be consistent with that of ordinary chondrite meteorites except for a depletion in S. Such a composition would be consistent with spatially resolved, visible and near-infrared (NIR) spectra of the surface. Gamma-ray spectra from the surface show Fe to be depleted from chondritic values, but not K. Eros is not a highly differentiated body, but some degree of partial melting or differentiation cannot be ruled out. No evidence has been found for compositional heterogeneity or an intrinsic magnetic field. The surface is covered by a regolith estimated at tens of meters thick, formed by successive impacts. Some areas have lesser surface age and were apparently more recently disturbed or covered by regolith. A small center of mass offset from the center of figure suggests regionally nonuniform regolith thickness or internal density variation. Blocks have a nonuniform distribution consistent with emplacement of ejecta from the youngest large crater. Some topographic features indicate tectonic deformations. Several regional-scale linear features have related orientations, suggesting a globally consolidated internal structure. Structural control of crater shapes hints that such internal structure is pervasive. From the bulk density, inferred composition, and evidence for global structure, Eros is interpreted to be largely intact but extensively fractured.

1. INTRODUCTION

The Near Earth Asteroid Rendezvous (*NEAR*) spacecraft was launched on February 17, 1996, and performed the first flyby of a C-type main-belt asteroid, 253 Mathilde, on June 27, 1997 (*Veverka et al.,* 1997b; *Yeomans et al.,* 1997b). *NEAR* performed a flyby of Eros on December 23, 1998 (*Yeomans et al.,* 1999; *Veverka et al.,* 1999a), and on February 14, 2000, *NEAR* entered orbit around Eros, becoming the first spacecraft to orbit an asteroid. The spacecraft was then renamed *NEAR Shoemaker* in honor of Eugene M. Shoemaker (1928–1997). After successfully completing its year-long orbital mission, *NEAR Shoemaker* became the first spacecraft to land on an asteroid. On February 12, 2001, it touched down softly on Eros, close to the southeastern edge of the saddle-shaped depression Himeros at 37.2°S by 278.4°W (all names of features on Eros are those proposed by the *NEAR* Science Team to the IAU; see appendix).

NEAR Shoemaker was a three-axis stabilized spacecraft that carried a six-instrument scientific payload. This paper summarizes results obtained by the NEAR Science Team using a multispectral imager (MSI), a near-infrared spectrometer (NIS), a laser rangefinder (NLR), an X-ray spectrometer (XRS), a γ-ray spectrometer (GRS), and a magnetometer (MAG). In addition, *NEAR Shoemaker* included a radio science investigation (RS) using the spacecraft telecommunications system. The scientific background and expected results of these investigations on *NEAR* were summarized in a special issue of the *Journal of Geophysical Research* (*Cheng et al.,* 1997; *Veverka et al.,* 1997a; *Trombka et al.,* 1997; *Zuber et al.,* 1997; *Acuña et al.,* 1997; *Yeomans et al.,* 1997a).

In what follows, a brief overview of the spacecraft, instruments, and mission as flown is presented, after which the science background and original objectives of the mission are summarized. Next, a selective review of asteroid science pertinent to *NEAR* mission objectives is given to provide context. Then a summary of results at Mathilde is given, followed by a summary of Eros results. Some outstanding issues and directions for future work are discussed in the conclusion.

2. *NEAR SHOEMAKER* SPACECRAFT

NEAR was a solar-powered, three-axis-stabilized spacecraft (*Santo et al.,* 1995) with a launch mass, including propellant, of 805 kg and a dry mass of 468 kg. The spacecraft was simple and highly redundant (Fig. 1). It used X-band telemetry to the NASA Deep Space Network. With a 70-m antenna, the data rates from Eros ranged from 17.6 to 26.5 kbps. Two solid-state recorders were accommodated with a combined memory capacity of 1.6 Gb. Spacecraft attitude was determined using a star camera, a fully redundant inertial measurement unit, and redundant digital Sun sensors. The propulsion subsystem was dual mode, using hydrazine as fuel for both monopropellant and bipropellant thrusters. Attitude was controlled by a redundant set of four reaction wheels or by the thruster complement to within

1.7 mrad. *NEAR*'s line-of-sight pointing stability was within 20 μrad over 1 s, and postprocessing attitude knowledge was within 130 μrad.

NEAR contained six scientific instruments, which are detailed in the next section. The MAG was mounted on top of the high-gain antenna feed, where it was exposed to the minimum level of spacecraft-generated magnetic fields. The remaining instruments (MSI, NIS, XRS, GRS, and NLR) were mounted on the aft deck (Fig. 1), all on fixed mounts, and were coaligned to view a common boresight direction. The NIS had a scan mirror that allowed it to look 110° away from the common boresight. Key properties of the mission design permitted the use of this fixed spacecraft geometry. Throughout most of the orbital rendezvous with Eros, the angle between the Sun and the Earth as seen from the spacecraft remained less than ~30°. In addition, the mission aphelion was reached during cruise. Hence, if the solar panels were sufficiently large to sustain *NEAR* at aphelion, there was sufficient power margin at Eros for the spacecraft to pull its solar panels 30° off full illumination to point the HGA at Earth. Moreover, the rendezvous orbit plane was maintained so that the orbit normal pointed approximately at the Sun. In this case, as *NEAR* orbited Eros, it was able to roll around the HGA axis so as to keep the instruments pointed at the asteroid. (The instruments were usually pointed away from the asteroid when the HGA was used to downlink to Earth.) This mode of operation motivated the requirement for onboard data storage. With onboard image compression, *NEAR* could store more than 1000 images and downlink them within 10 h at its maximum data rate of 26.5 kbps.

3. INSTRUMENTS

A brief summary of instrument characteristics is given in this section (Fig. 2). Full descriptions of each instrument's design and science operations can be found in a special issue of *Space Science Reviews* (vol. 82, 1997). Additional information on results of inflight calibrations have been published and are given as the second members of the paired citations in this section.

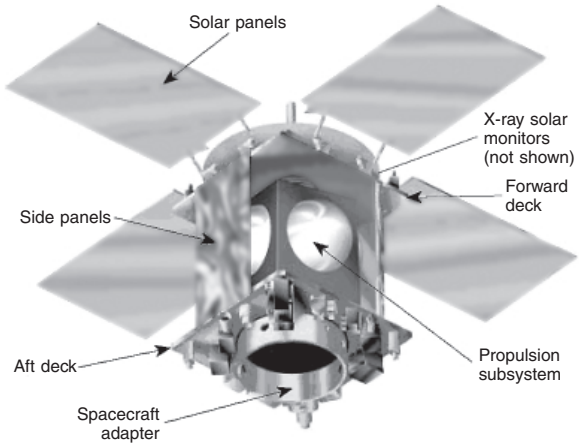

Fig. 1. The *NEAR Shoemaker* spacecraft, showing the aft deck where all instruments except the magnetometer and the X-ray solar monitors were mounted. Side panels have been removed to show the propulsion subsystem.

All data from the *NEAR* mission were downlinked to the NASA Deep Space Network and then forwarded to the Mission Operations Center (MOC) at the Johns Hopkins University's Applied Physics Laboratory (APL) (*Heeres et al.,* 1997). Doppler and ranging data from the spacecraft were analyzed by the *NEAR* navigation team at the Jet Propulsion Laboratory (JPL). The entire spacecraft telemetry stream, including spacecraft and instrument housekeeping data, navigation data, and all science data, was forwarded to the APL MOC together with the radiometric Doppler and range data. The spacecraft telemetry stream was then passed to the Science Data Center at APL, which supported the data analysis and archiving activities. *NEAR* data were released over the Internet at http://near.jhuapl.edu/. All *NEAR* data have been archived in the NASA Planetary Data System. The total archived data volume amounted to approximately 212 GB.

3.1. Multispectral Imager (MSI)

The main goals of the MSI (*Hawkins et al.,* 1997; *Murchie et al.,* 1999, 2002a) were to determine the shape of Eros and map the mineralogy and morphology of features on its surface at high spatial resolution. MSI was a 537 × 244-pixel charge-coupled device camera with five-element radiation-hardened refractive optics. It covered the spectral range from 0.4 to 1.1 μm, and it had an eight-position filter wheel (Table 1). Seven narrow-band filters were chosen to discriminate the major Fe-bearing silicates present (olivine and pyroxene); the eighth, broadband filter provided higher sensitivity for starfield exposures to enhance optical navigation. The camera had an FOV of 2.93° × 2.26° and a pixel resolution of 96 × 162 μrad. It had a maximum framing rate of 1/s with images digitized to 12 bits and a dedicated digital processing unit with an image buffer in addition to both lossless and lossy onboard image compression (lossless compression causes no loss of information, whereas lossy compression yields a more compact dataset with loss of information).

3.2. Near-Infrared Spectrometer (NIS)

The NIS (*Warren et al.,* 1997; *Izenberg et al.,* 2000) measured the spectrum of sunlight reflected from Eros in the NIR range from 0.8 to 2.5 μm to determine the distribution and abundance of surface minerals like olivine and pyroxene. This grating spectrometer dispersed the light from the slit FOV (0.38° × 0.76° in its narrow position and 0.76° × 0.76° in the wide position) across a pair of passively cooled one-dimensional array detectors. A 32-channel Ge array covered the lower wavelengths, with channel centers at 0.82–1.49 μm with a 0.022-μm spacing between channels. A 32-channel In/Ga-As array covered longer wavelengths, with channel centers at 1.37–2.71 μm with a 0.043-μm spacing between channels. Due to the configuration of the optics and

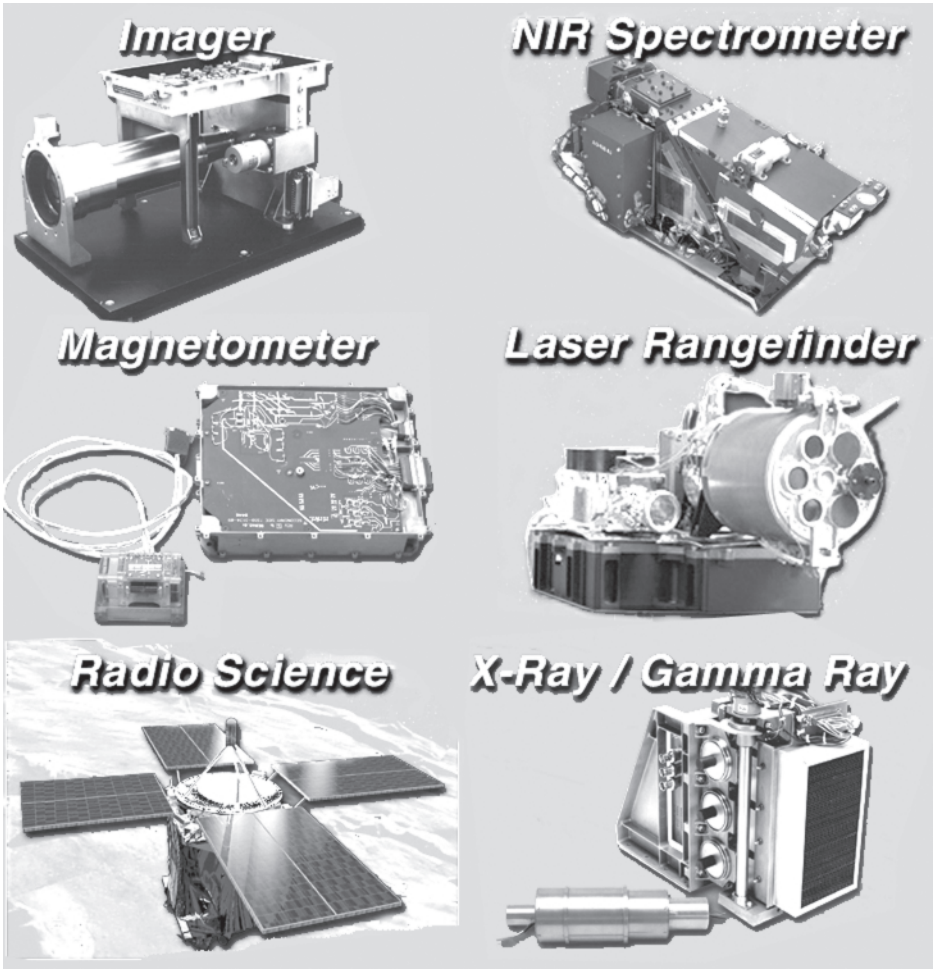

Fig. 2. The *NEAR Shoemaker* instruments and radio science experiment. The high-gain antenna is the circular dish centered amidst the four solar panels.

TABLE 1. NEAR MSI filter positions (*Murchie et al.,* 1999).

Filter Number	Nominal Center (nm)	Nominal Width (nm)	Effective Center (nm)	Effective Width (nm)
2	450	50	462	23
1	550	30	554	24
0	700	200	700	133
3	760	20	755	19
5	900	40	900	33
4	950	40	951	38
6	1000	50	996	44
7	1050	80	1033	51

the sensitivity of this array, useful measurements were acquired over the wavelength range 1.5–2.5 μm. NIS had a scan mirror that enabled it to step across the range from 30° forward of the common boresight to 110° aft, in 0.4° steps. Spectral images were built up by a combination of scan mirror and spacecraft motions. In addition, the NIS had a gold calibration target that viewed at the forward limit of the mirror's scan to provide inflight calibration of instrument stability.

3.3. X-Ray Spectrometer (XRS)

The XRS (*Goldsten et al.,* 1997; *Starr et al.,* 2000) was an X-ray fluorescence spectrometer that measured characteristic X-ray line emissions excited by solar X-rays from major elements in the asteroid's surface. It covered X-rays from 1 to 10 keV using three gas-proportional counters. The balanced, differential filter technique was used to separate the closely spaced Mg, Al, and Si lines below 2 keV. The gas-proportional counters directly resolved higher-energy line emissions from Ca and Fe. A mechanical collimator gave the XRS a 5° field-of-view (FOV), yielding a spatial resolution as fine as 2 km in the low orbits. The XRS also included a solar monitor to measure continuously the incident spectrum of solar X-rays, using both a gas-proportional counter and a high-spectral-resolution Si X-ray detector. The XRS performed inflight calibration using a calibration rod with Fe^{55} sources that could be rotated into or out of the detector FOV.

3.4. Gamma-Ray Spectrometer (GRS)

The GRS (*Goldsten et al.,* 1997; *Evans et al.,* 2000) detected characteristic γ-rays from 0.3 to 10 MeV emitted

from the asteroid surface. Some of these emissions were excited by cosmic rays and some arose from natural radioactivity in the asteroid. The GRS used a body-mounted, passively cooled NaI scintillator detector with a bismuth germanate anticoincidence shield that defined a 45° FOV. Abundances of several important elements such as K, Si, O, and Fe were measured.

3.5. *NEAR* Laser Rangefinder (NLR)

The NLR (*Cole et al.,* 1997; *Cheng et al.,* 2000) was a laser altimeter that measured the distance from the spacecraft to the asteroid surface by sending out a short burst of laser light and then recording the time required for the signal to return from the asteroid. It used a Cr-Nd-YAG solid-state laser and a compact reflecting telescope. It sent a small portion of each emitted laser pulse through an optical fiber of known length and into the receiver, providing a continuous inflight calibration of the timing circuit. The ranging data were used to construct a global shape model and a global topographic map of Eros with horizontal resolution of ~400 m. The NLR also measured detailed topographic profiles of surface features on Eros with a best spatial resolution <5 m.

3.6. Magnetometer

The fluxgate magnetometer (*Lohr et al.,* 1997; *Acuña et al.,* 2000) used ring core sensors made of highly magnetically permeable material. It searched for any intrinsic magnetic fields of Eros. The previous *Galileo* flybys of the S-type asteroids Gaspra and Ida yielded evidence that both of these bodies are magnetic, although this evidence is ambiguous (*Kivelson et al.,* 1993). If Eros were as magnetized as typical meteorites, its magnetic field would have been easily measured. Discovery of an intrinsic magnetic field at Eros would have yielded important insights about its thermal and geological history.

3.7. Radio Science

In addition to the six instruments, the coherent X-band transponders (*Yeomans et al.,* 1997a) were used to conduct a radio science investigation by measuring the Doppler shift from the spacecraft's radial velocity component relative to Earth. Accurate measurements of the Doppler shift and the range to Earth as the spacecraft orbited Eros allowed mapping of the asteroid's gravity field. In conjunction with MSI/NIS and NLR data, gravity determinations were combined with global shape and rotation data to constrain the internal density structure of Eros and search for heterogeneity.

4. THE *NEAR* MISSION

The *NEAR* spacecraft was launched on February 17, 1996, by a Delta II 7925 launch vehicle (Fig. 3). The Mathilde encounter occurred on June 27, 1997, one week before the deep space maneuver. The Earth swingby (*Izenberg and Anderson,* 1998) occurred on January 23, 1998, retargeting the *NEAR* spacecraft to Eros. After a main rocket engine abort on December 20, 1998, a flyby of Eros was performed on December 23, 1998, and the Eros rendezvous was rescheduled for February 14, 2000, when orbit insertion occurred. On February 12, 2001, *NEAR* accomplished a soft landing on Eros.

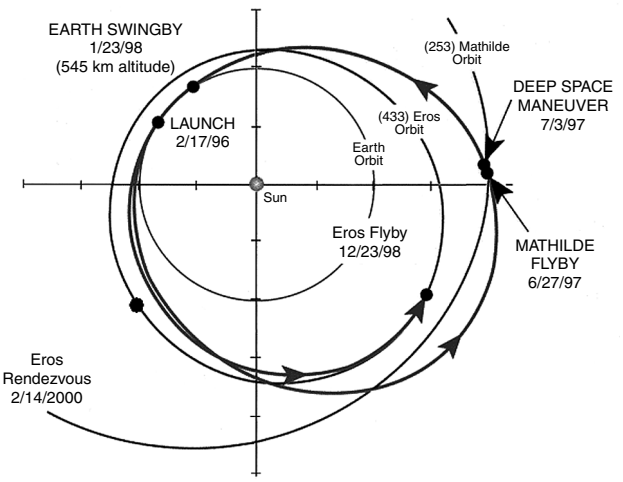

Fig. 3. Heliocentric trajectory of *NEAR Shoemaker,* with vernal equinox to the right, and orbits of Earth, Mathilde, and Eros. After the Eros flyby, *NEAR Shoemaker* followed the orbit of Eros to within the accuracy of this figure.

5. EROS OPERATIONS

Beginning in January 2000, a sequence of small maneuvers decreased the relative velocity between *NEAR* and Eros to only 5 m/s. On February 14, 2000, *NEAR* performed a flyby of Eros on its sunward side at a distance as low as 130 km. In addition to gathering spectra at an optimal illumination geometry, this first pass provided improved estimates of the asteroid's physical parameters (Table 3), such as a mass determination to 1% accuracy, identification of surface landmarks, and an improved estimate of Eros' spin vector. As the spacecraft maneuvered closer to Eros, the mass, moments of inertia, gravity harmonics, spin state, and landmark locations were determined with increasing precision. The year-long prime science phase at Eros began on February 14, 2000. During this phase, *NEAR* operated in a series of orbits that come as close as 3 km to the asteroid's surface, culminating with a soft landing on February 12, 2001. The evolution of low-altitude orbits around Eros was strongly influenced by its irregular gravity field. For some possible orbital conditions, the spacecraft would have crashed into Eros in a few days. Safe orbital operations required close coordination between the science, mission design, navigation, and mission operations teams (*Landshof and Cheng,* 1995).

Figure 4 depicts the *NEAR* spacecraft in a low-altitude, circular orbit around Eros as viewed by an observer on the Sun. This is a convenient reference frame to show *NEAR*'s

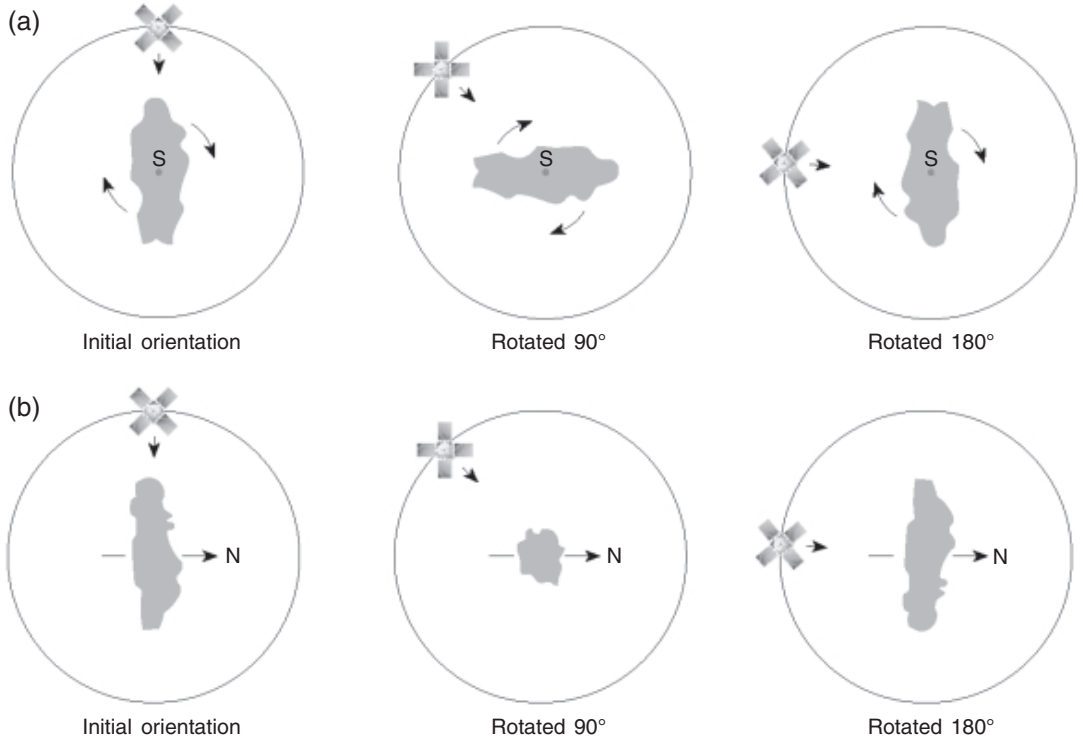

Fig. 4. Examples of orbital geometries at Eros as viewed from the Sun, at an initial rotational phase of Eros (left), after 90° rotation (center), and after 180° rotation (right). The small arrow by the spacecraft shows the instrument boresight. **(a)** Spacecraft is in retrograde equatorial orbit, and the south pole of Eros is marked by S. **(b)** Spacecraft is in polar orbit, and the spin axis of Eros is shown.

orbit because the orbital plane was controlled so that it was always within 30° of a plane perpendicular to the Sun-Eros line. In this orbital geometry, *NEAR*'s fixed solar panels were oriented toward the Sun. The science instruments were pointed at Eros' surface by rolling the spacecraft around its high-gain antenna axis as it orbited the asteroid. Two fundamentally different orbital geometries are shown in Fig. 4. In Fig. 4a, Eros' rotation axis is aligned with the Sun-Eros line. Its south pole points toward the Sun, which means that its northern hemisphere is shadowed. In this case, which applied during roughly the last two months of the orbital phase, the spacecraft orbit was retrograde and approximately equatorial. Earlier in the orbital mission, the asteroid's rotation axis was roughly perpendicular to the Sun-Eros line, and the spacecraft orbit was approximately polar as shown in Fig. 4b. This was the geometry that prevailed roughly from May through August 2000.

Because of the changing orbital geometry, coverage of Eros' surface by the instruments varied throughout the orbital mission. The subsolar point lay in the northern hemisphere early in the mission, crossing to the southern hemisphere on June 26, 2000, and remaining in the south thereafter. All areas on the asteroid were observed many times under diverse illumination conditions and viewing geometries.

The mission profile at Eros is summarized in Fig. 5. To simplify science operations, the orbital mission was divided into distinct phases (*Landshof and Cheng,* 1995). The highest-priority science varied by mission phase, because of the changing orbital geometry. While in orbits at 100 km from the center of Eros or higher, the highest-priority science was global mapping by MSI. In orbits at 50 km or lower, the highest-priority science was compositional measurement by XRS/GRS. A two-week period was allocated to altimetry

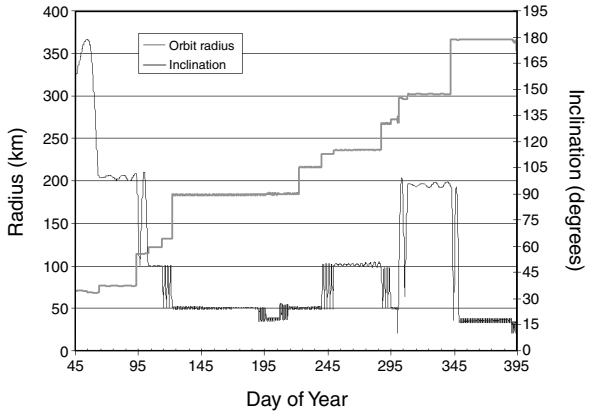

Fig. 5. Eros orbital phase as flown. The thin curve is the orbit radius (left axis) measured from the center vs. day of year 2000. The thick curve is the orbital inclination (right axis), where inclination <90° is prograde and inclination >90° is retrograde. The orbit was retrograde in the second half of the orbital phase. The figure extends from February 14, 2000, through January 29, 2001.

by NLR at the start of the 50-km polar orbits in May 2000. First detection of Eros by NLR occurred at a range of 290 km. *NEAR* spent more than 150 d in orbits at 50 km or less from the center of Eros, plus two additional weeks on the surface acquiring GRS data. In general, all instruments acquired data in all mission phases, except that NIS ceased operating on May 13, 2000, and only GRS was operated on the surface of Eros.

The rendezvous burn sequence was designed to put *NEAR* into an initial slow flyby trajectory past Eros, taking the spacecraft through a zero solar phase angle (Sun-asteroid-spacecraft angle) at a miss distance of 200 km. This flyby enabled NIS to obtain critical science observations. Since the nominal rendezvous orbit plane was kept near the Eros terminator (plane dividing the dayside from the nightside), most of the orbital observations were obtained at large phase angles >60° that were favorable for imaging but unfavorable for IR spectral mapping. The low-phase flyby on February 14, 2000, provided an important opportunity for NIS to obtain infrared spectral maps of the entire illuminated surface (the northern hemisphere) under optimal lighting conditions with minimum shadowing. Since the NIS failed on May 13, 2000, execution of a second low-phase flyby over the southern hemisphere of Eros was canceled. Instead, a low-altitude flyover to within 6 km of the surface was performed on October 26, 2000. The two weeks after the timespan of Fig. 5 were devoted mainly to preparations for the descent to the surface on February 12, 2001.

An optical search for satellites of Eros was performed during the approach to Eros before the initial flyby. No satellites were discovered at Eros (*Veverka et al.,* 2000), with a sensitivity limit of 20 m diameter for an albedo equal to that of Eros.

6. SCIENCE BACKGROUND

The vast majority of known asteroids is found in the main asteroid belt between the orbits of Mars and Jupiter, but those that come within 1.3 AU of the Sun are known as near-Earth asteroids (NEAs). The *NEAR* target 433 Eros is the second largest of the NEAs. The orbits of these dynamically young bodies have evolved on 100-m.y. timescales because of collisions, the Yarkovsky effect (reaction force from anisotropic emission of thermal radiation), and gravitational interactions with planets (*Bottke et al.,* 2000). The present-day orbits of NEAs do not indicate where they formed. NEAs are believed to originate from the main belt, and their orbital evolution can cause them to impact the Sun, collide with a terrestrial planet, or be ejected from the solar system. More than 1500 near-Earth asteroids are known as of October 2001, of which more than 238 have orbits determined well enough to be numbered. The NEAs appear to represent a broad sample of the main-belt population.

Before *NEAR,* knowledge of the nature of asteroids came from three sources: Earth-based remote sensing, data from the *Galileo* spacecraft flybys of the two main-belt asteroids 951 Gaspra and 243 Ida, and laboratory analyses of meteorites. Most meteorites are believed to be collisional fragments of asteroids (a few come from the Moon and from Mars), but they may represent a biased and incomplete sampling of the materials actually found in and on near-Earth asteroids. Firm links between meteorite types and asteroid types have been difficult to establish (*Gaffey et al.,* 1993a). The uncommon HED basaltic achondrite meteorites have been linked by visible and NIR reflectance measurements to the V-type asteroids (*McCord et al.,* 1970; *Binzel and Xu,* 1993).

However, the links between asteroids and meteorites are controversial in several ways. Foremost are the questions of whether and how the most common meteorite types (ordinary chondrites, or OCs) may be linked to the most common asteroid types (S asteroids) in the inner part of the asteroid belt (*Bell et al.,* 1989; *Gaffey et al.,* 1993b). Gaspra and Ida, which were visited by *Galileo,* and the *NEAR* target 433 Eros, are all S asteroids — a diverse class of objects containing the silicate minerals olivine and pyroxene plus an admixture of Fe/Ni metal. Some S asteroids appear to be fragments of bodies that underwent substantial melting and differentiation, whereas others may consist of primitive materials like OCs that underwent little or no melting and that may preserve characteristics of the solid material from which the inner planets accreted. Few asteroids have been found to be clear spectral analogs for OCs, compared to the numbers of asteroids that may represent differentiated cores and crusts (*Bell et al.,* 1989; *Xu et al.,* 1995). Many authors have suggested that a "space-weathering process," due to micrometeorite bombardment and/or radiation processing, may suitably alter spectral properties of optical surfaces on asteroids (*Chapman,* 1996) so that OC materials on asteroids are not recognized spectrally.

The *Galileo* flybys of Gaspra and Ida provided the first high-resolution images of asteroids, revealing complex surfaces covered by craters, fractures, grooves, and subtle color variations (*Belton et al.,* 1992, 1994). *Galileo* also discovered the satellite Dactyl of Ida (*Belton et al.,* 1996), which is a member of the Koronis family. The NIR spectrum of Gaspra indicates a high olivine abundance such that it is inferred to be a fragment of a differentiated body, but Ida and Eros display IR spectra that may be consistent with a silicate mineralogy like that in OCs (*Chapman,* 1996; *Murchie and Pieters,* 1996). The *Galileo* instrument complement did not include any capability to measure elemental composition.

Another fundamental question deals with the collisional history of small bodies in the early solar system, when the terrestrial planets formed and when disruption by violent impacts competed with accretion from gentler collisions. The question is whether asteroids the size of Eros must have been battered into an agglomeration of much smaller components bound mostly by gravity (that is, a rubble pile), or are instead intact collisional fragments from larger parent bodies ("collisional shards"). A collisional shard would be a globally consolidated body with appreciable shear and/or tensile strength, for which self-gravitation would be rela-

tively unimportant. For Gaspra, the faceted shape and the presence of grooves may hint at such a picture (*Thomas et al.,* 1994). However, an alternative picture is that asteroids the size of Eros were thoroughly broken up without being dispersed (or possibly, Eros reaccreted), so they would now be rubble piles (e.g., *Davis et al.,* 1994; *Melosh and Ryan,* 1997). Some small asteroids rotate so rapidly that they must be monolithic (e.g., *Ostro et al.,* 1999), but the vast majority of asteroids larger than 0.2 km have rotation periods shorter than 2 h, suggesting that most of these larger bodies are rubble piles (*Pravec and Harris,* 2001).

The *NEAR* mission made the first comprehensive, spatially resolved measurements of the geology, mineralogy, and elemental composition of an S-type asteroid. Table 2 lists a set of science questions that were originally formulated in 1985 by the Near Earth Asteroid Rendezvous Science Working Group (*NEAR Science Working Group,* 1986). The present *NEAR* mission was designed to address these questions. The table identifies the *NEAR* instruments whose measurements addressed these questions and provides a summary of principal findings. As can be seen in Table 2, the *NEAR* findings exceeded and/or defied expectations in many cases.

7. MATHILDE FLYBY

The *NEAR* encounter with 253 Mathilde is significant because it was the first spacecraft encounter with a C asteroid, a completely different type of object from the S asteroids visited earlier by *Galileo* and explored later by *NEAR*. The dark C asteroids are the most common type in the central portion of the main belt of asteroids. Their carbonaceous composition is inferred from the spectral similarity of C asteroids and the carbonaceous chondrite meteorites. The visible spectrum of Mathilde in particular (*Binzel et al.,* 1996) is similar to the spectra of 1 Ceres and 2 Pallas (the two largest asteroids), but Mathilde has no 3-μm water absorption feature; its NIR spectrum is consistent with heated (to 900°C) carbonaceous chondrites or black chondrites (*Rivkin et al.,* 1997). The nature and origins of the dark, primitive asteroid types (B, C, F, G, P, D, etc.), and their relationships to the comets and the dark objects in the satellite systems of the outer planets are among the most important unresolved issues in solar-system exploration.

Apart from its importance as the first example of the C asteroids to be explored, Mathilde is extremely slow rotating (*Mottola et al.,* 1995). Its 17.4-d period is the third-

TABLE 2. *NEAR* science closure.

Science Question	Instruments	Summary Of Principal Findings
What are the morphological and textural characteristics of the asteroid surface, and how do they compare with those on larger bodies?	MSI, NLR	Tectonic features; pervasive covering of tens-of-meters thick regolith; large spatial variations in density of large craters; dearth of small craters; high boulder densitites; ponded deposits of regolith emplaced in fluidized form.
What is the elemental composition of the asteroid?	XRS, GRS	For areas observed by XRS, elemental composition was consistent with ordinary chondrites, except for sulfur depletion; GRS spectra at landing site suggest depletion in iron from chondritic values, but K chondritic.
What is the mineralogical composition of the asteroid?	NIS, MSI	Mineral composition is consistent with ordinary chondrite or similar material.
Is there evidence of compositional or structural heterogeneity?	MSI, NIS; NLR; RS; XRS	Structural control of crater formation; evidence for faulting; no evidence for compositional heterogeneity.
Is the asteroid a solid fragment of a larger parent body or a rubble pile?	MSI, NIS; NLR; RS; XRS	Eros largely intact but deeply fractured, most likely a fragment of a larger parent body; alignments of linear features suggest through-going internal structures.
Is the asteroid's precursor body(ies) primitive or differentiated?	XRS, GRS; NIS, MSI	Eros precursor was primitive, but some degree of metamorphism or partial melting not ruled out.
Is there evidence of past or present cometary activity?	MSI; NLR	None found.
Is the asteroid related to a meteorite type or types?	XRS, GRS; NIS, MSI	Eros may be similar to ordinary chondrites, but definitive relationship to petrologic group not established.
Does an intrinsic magnetic field exist? What is it like?	MAG	No intrinsic magnetic field found.
Does the asteroid have any satellites, and how might they compare with Eros?	MSI	No satellites found.

TABLE 3. Four asteroids visited by spacecraft.

Asteroid	Dates Visited by Spacecraft	Heliocentric Orbit: a, e, i	Ellipsoidal Diameters	Density (g cm^{-3})	Rotation Period
951 Gaspra	10/29/91 by *Galileo*	a = 2.21 AU, e = 0.173, i = 4.10°	19 km × 12 km × 11 km	?	7.04 h
243 Ida	9/29/93 by *Galileo*	a = 2.86 AU, e = 0.046, i = 1.14°	59.8 km × 25.4 km × 18.6 km	2.6 ± 0.5	4.63 h
253 Mathilde	6/27/97 by *NEAR*	a = 2.65 AU, e = 0.265, i = 6.71°	66 km × 48 km × 46 km	1.3 ± 0.2	17.4 d
433 Eros	12/23/1998; and 2/14/2000 through 2/28/2001 by *NEAR*	a = 1.46 AU, e = 0.223, i = 10.8°	34.4 km × 11.2 km × 11.2 km	2.67 ± 0.03	5.27 h

References: *Belton et al.* (1992, 1996); *Mottola et al.* (1995); *Yeomans* (1995); *Yeomans et al.* (1997b, 2000); *Veverka et al.* (1999b, 2000); *Zuber et al.* (2000).

longest known and is at least an order of magnitude longer than that of typical asteroids. The origin of these very slow rotation states is puzzling (*Harris,* 1994).

Table 3 shows key characteristics of four asteroids visited by spacecraft so far, including the diameters of best-fit ellipsoids, which give a rough indication of size (the shapes are not well described by ellipsoids in any of the four cases). Mathilde is the largest of the four, by far the slowest rotating and the only C asteroid. *NEAR*'s encounter with Mathilde took place under difficult conditions: at an approach phase angle of 140° and a distance of 1.99 AU from the Sun, where the available power from the spacecraft's solar panels was reduced to about 25% of its maximum mission level. The solar panels could not be pointed more than 50° away from the optimal solar direction because of available power, and only the MSI could be operated during the encounter (*Veverka et al.,* 1997b, 1999b). However, spacecraft tracking data for the radio science experiment were obtained for a mass determination (*Yeomans et al.,* 1997b).

The entire imaging sequence was accomplished in about 25 min, during which 534 images were obtained. Closest approach was 1212 km and the flyby speed was 9.93 km/s. The whole illuminated portion of the asteroid was imaged in color at about a 500-m/pixel resolution after closest approach at phase angles near 40°. The best partial views, acquired at higher phase angles, had a resolution of 200–350 m/pixel. At closest approach, the imager was accurately targeted to the center of Mathilde, but happened to view the deeply shadowed interiors of giant craters, which were completely dark (*Veverka et al.,* 1999b).

8. MATHILDE RESULTS

The *NEAR* flyby obtained the first direct mass determination of an asteroid (*Yeomans et al.,* 1997b). The measured mass of 1.03×10^{20} g and estimated volume of 78,000 km^3 imply a density of 1.3 ± 0.2 g cm^{-3}. The volume must be estimated because only one face of Mathilde could be imaged during the 25-min *NEAR* flyby. The inferred density was unexpectedly low, half or less than that of carbonaceous chondrite meteorites that are the closest spectral analogs, and it implies a high porosity of 50% or more (*Veverka et al.,* 1997b, 1999b). No natural satellite of Mathilde was found. The surface of Mathilde is heavily cratered, with at least five giant craters whose diameter is comparable to the 26.5-km mean radius of Mathilde itself. The areal density of smaller craters <3 km diameter is approximately at equilibrium, similar to that of 243 Ida. However, the presence of the five giant craters was a surprise, because impacts of the magnitude required to make such large craters are about the largest that can be survived without disruption of the target (*Greenberg et al.,* 1996). The mere existence of giant craters on Mathilde was not surprising, but the presence of five giant impacts on a single face of the asteroid was remarkable in that the giant craters did not disrupt one another. Finally, Mathilde proved to be highly uniform in both color and albedo. Mathilde was known from groundbased observations to be a C-type asteroid, and therefore dark and spectrally neutral, but the ground observations could not rule out the possibility of spectrally distinct regions. The *NEAR* observations revealed no evidence of any albedo or spectral variations, implying a homogeneous composition. The measured geometric albedo of 0.043 ± 0.005 was consistent with telescopic observations [*Clark et al.* (1999); improved calibration is given by *Murchie et al.* (2002a)].

Mathilde's low density implies a high porosity and is consistent with a rubble-pile structure. This is clearly a significant result for Mathilde's geologic history, but it is unclear whether Mathilde's porosity is microscopic or macroscopic. The nature and distribution of voids within the interior also remain unclear. The porosity of Mathilde may be primordial; that is, Mathilde may have originally accreted as a po-

rous structure and survived as such to the present. Alternatively, the structure may be an agglomerate of larger fragments, subsequently accreted to form Mathilde. For example, Mathilde may have been thoroughly disrupted by impacts but not dispersed. In this case, macroscopic voids would be expected, possibly in addition to microscopic porosity.

The *NEAR* observations provide important clues to the nature of Mathilde. No ejecta blankets, and no ejecta blocks, have been identified on Mathilde, although blocks larger than 300 m are not expected (*Thomas et al.,* 1999); the resolution limit was approximately 500 m for most of the surface that could be imaged. If Mathilde accreted fragments of diverse parent bodies, these must have had remarkably uniform albedos and colors, or else the fragments must be smaller than ~500 m. Evidence for structure has been reported from images; there are polygonal craters, a 20-km-long marking interpreted as a scarp and a sinuous linear feature that may be an exposed layer (*Thomas et al.,* 1999).

The giant craters provide additional clues to Mathilde's history and nature. Mathilde's porosity makes it more difficult to crater and enhances the likelihood of survival of giant impacts (*Chapman et al.,* 1999; *Cheng and Barnouin-Jha,* 1999; *Davis,* 1999). Porosity causes efficient shock damping, and collapse of pore space rapidly dissipates impact energy. Moreover, roughly half of all impacts are more oblique than 45°. An oblique impact generates lower peak pressure and lower peak strain rates than a normal impact that creates the same-sized crater, so oblique impacts are also less likely to disrupt a target. If account is taken of oblique impacts and of Mathilde's porosity, then the probability of making a giant crater is 2.1–2.6× more than the probability of disruption (*Cheng and Barnouin-Jha,* 1999). Recent laboratory experiments on cratering in highly porous targets (*Housen et al.,* 1999) have shown that the crater volume in this case is produced mainly by target compression rather than excavation and that ejecta volumes are reduced. These results may explain not only how Mathilde survived so many giant impacts, but also how a giant crater can be emplaced practically adjacent to another without disrupting it (Fig. 6). Mathilde's high porosity is key to understanding its collisional history, but its structural features, such as the aforementioned scarp, and its polygonal craters indicate that it is not completely strengthless and that at least one of its structural components appears coherent over a few tens of kilometers.

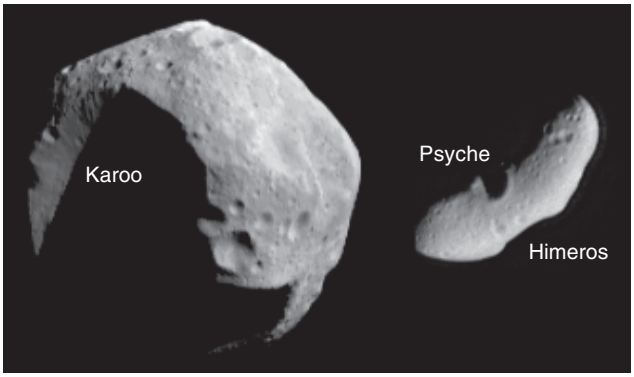

Fig. 6. Asteroids visited by *NEAR*: Mathilde (left) and Eros (right). The images are in the approximate relative scale, but the C asteroid Mathilde is much darker than shown relative to Eros. On Mathilde the giant crater Karoo, diameter 33 km, is marked. On Eros, the 5-km-crater Psyche is at the terminator and is labeled. At the bright limb of Eros, the saddle-shaped depression Himeros is labeled.

9. EROS RESULTS

The 1998 *NEAR* flyby of Eros yielded determinations (*Veverka et al.,* 1999a; *Yeomans et al.,* 1999) of the mass $(7.2 \pm 1.8) \times 10^{15}$ kg and density (2500 ± 800) kg m^{-3}. The size and rotation pole of Eros were found to be consistent with previous groundbased determinations. These data greatly enhanced the Eros orbital mission as actually flown, by facilitating planning and allowing earlier approach at low altitude. For reference, updated values of the mass and density after additional orbital measurements (*Yeomans et al.,* 2000) are $(6.687 \pm 0.003) \times 10^{15}$ kg and (2670 ± 30) kg m^{-3}.

Eros' average density of 2.67 g/cc is less than the average bulk density of ordinary chondrite meteorites as measured in the laboratory (*Wilkison et al.,* 2001), indicating that bulk Eros is significantly porous and/or fractured, but not to the same extent as Mathilde. The interior of Eros is nearly uniform in density, as inferred from its gravity field, which is within a few percent of that which would be expected from a uniform density object of the same shape (*Yeomans et al.,* 2000). There is a small center of mass offset from the center of figure that may be consistent with an underdense regolith layer of up to 100 m depth (*Zuber et al.,* 2000). Surface morphology clearly indicates the presence of a complex regolith (*Veverka et al.,* 2001a), inferred from the dearth of small craters (<100 m), the profusion of blocks and boulders in varying states of burial, and evidence for burial of small craters and mass wasting (*Cheng et al.,* 2002; *Thomas et al.,* 2002). Craters on Eros are typically shallower than craters of the same diameter on the Moon, consistent with an unconsolidated infill depth ranging from tens of meters to >100 m close to the largest impact craters (*Barnouin-Jha et al.,* 2001).

NEAR Shoemaker has shown that Eros is a consolidated body, not an agglomeration of smaller component bodies bound mostly by gravity (*Zuber et al.,* 2000). There are pervasive linear structural features: a variety of ridges, grooves, and chains of pits or craters (*Veverka et al.,* 2000) that display at least regionally coherent alignments over several kilometers across Eros. In a few cases, structural alignments have been demonstrated on global scales [e.g., between the 18-km-long ridge of Fig. 7 and a ridge system on the opposite face of Eros, southwest of Psyche as shown in Fig. 8 (*Thomas et al.,* 2002)]. Further evidence of structural strength is found from crater morphologies; many craters smaller than 1 km appear to be jointed and/or structurally controlled (*Prockter et al.,* 2002), although larger craters (e.g., Psyche in Fig. 6) are bowl-shaped. This finding is also consistent with a typical unconsolidated regolith

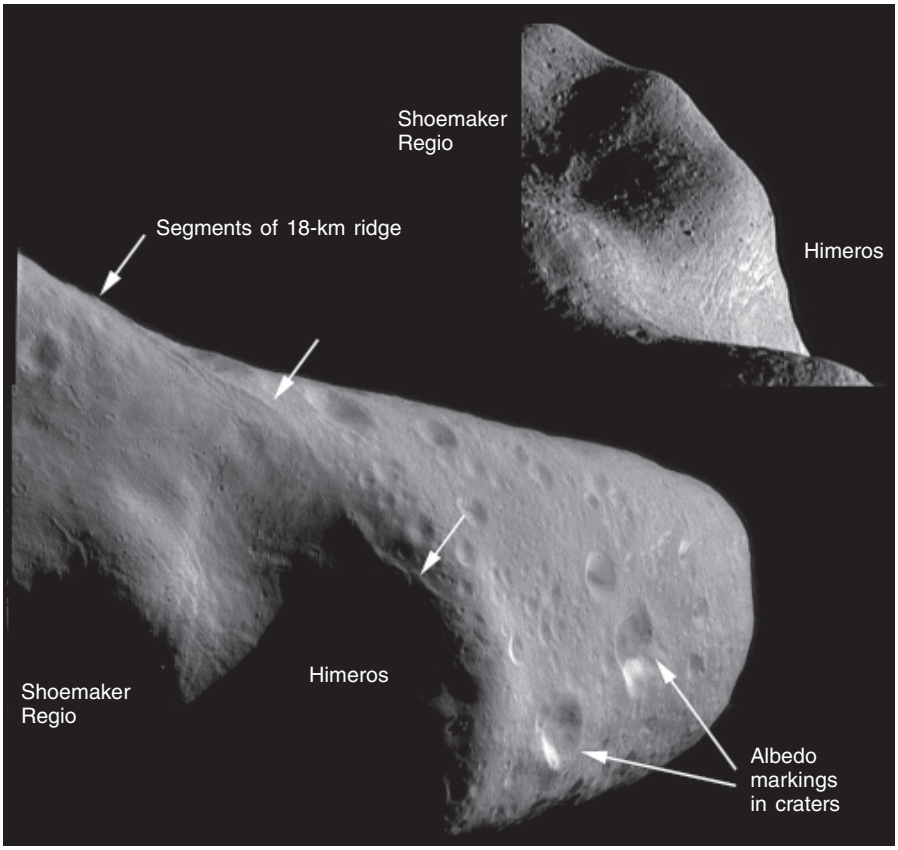

Fig. 7. Eros from 200-km orbit. At lower left, the saddle-shaped depression Himeros and the boulder-rich depression Shoemaker Regio are marked (these regions are in shadow). A portion of the 18-km-long ridge, which continues over the horizon, is marked with short arrows. The density of craters larger than 500 m is much greater outside Himeros and Shoemaker Regio. Systems of crosscutting grooves are seen in Himeros. Many crater walls exhibit bright and dark-albedo markings. The Sun is to the right. At upper right is another view of Himeros and Shoemaker Regio.

depth of <100 m. Additional evidence for a consolidated substrate is found in the presence of steep slopes over a few percent of the surface area that are well above expected angles of repose (*Zuber et al.,* 2000). Taken together, the linear structural features, the tectonic features such as the 18-km-long ridge, the jointed craters, and the indications of internal structural coherence, all suggest that Eros is a collisional fragment from a larger parent body. Nevertheless, throughgoing fractures may exist.

Most of Eros' surface is old and close to equilibrium saturation by craters >200 m (*Veverka et al.,* 2000; *Chapman et al.,* 2002), but some regions appear to be relatively young and extensively resurfaced. Blocks and boulders are ubiquitous but are not confined to gravitational lows; most may have originated from an impact that created Shoemaker Regio (*Thomas et al.,* 2001). The density of small craters (<100 m) is markedly depleted on Eros compared to the Moon, but the density of boulders is markedly enhanced, as illustrated in Fig. 9. The surface of Eros is extremely rough and exhibits a fractal structure from scales of a few meters up to hundreds of meters (*Cheng et al.,* 2001, 2002). Examples of downslope motion have been found on Eros, associated with steep slopes in crater walls (*Cheng et al.,* 2002). Bright albedo features are also associated with steep crater walls. The morphological and spectral properties of these features are consistent with a darkened, space-weathered material that slides down crater walls exposing brighter, less-weathered underlying material (*Murchie et al.,* 2002b; *Clark et al.,* 2001).

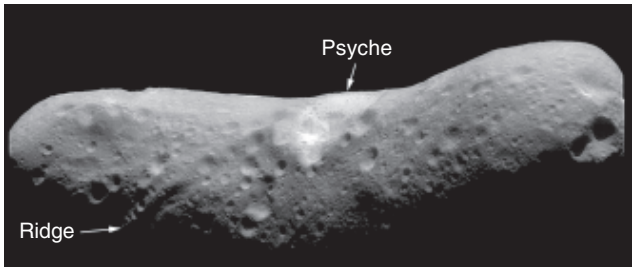

Fig. 8. Western face of Eros from 200-km orbit. Psyche crater is indicated, showing albedo markings on its walls. A prominent ridge, 140 m high, lies in roughly the same plane as the 18-km ridge of Fig. 7. Linear structural features indicate that Eros is a globally consolidated body.

Another unexpected finding at Eros was the discovery of extremely level, ponded deposits from high-resolution, low-altitude observations toward the end of the mission (*Veverka et al.,* 2001a,b; *Cheng et al.,* 2001; *Robinson et al.,* 2001). An example is shown in Fig. 9. The ponds are characterized by smooth, sharply bounded surfaces and are found in gravitational lows. Processes such as electrostatic levitation and seismic shaking from impacts have been discussed as possible means to mobilize fine particulates on the surface.

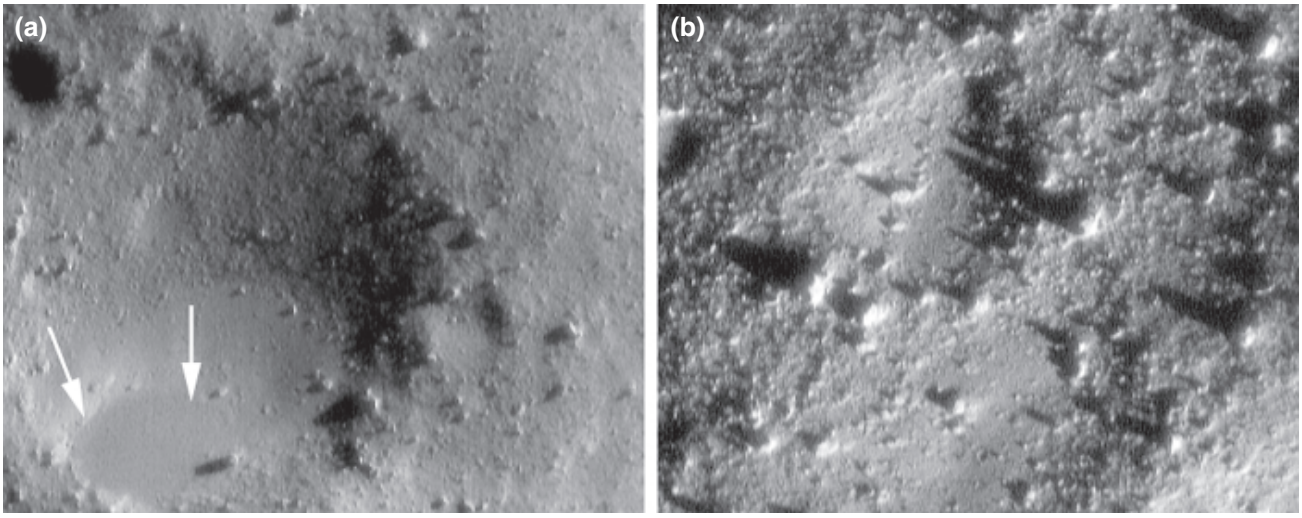

Fig. 9. Eros closeup. **(a)** Arrows indicate a pond within a degraded crater; this frame is about 250 m across. **(b)** Frame is about 150 m across and illustrates the high density of boulders and the paucity of small, fresh craters.

As summarized in Table 2, *NEAR* has shown that Eros is a primitive, intact object, not a rubble pile. The bulk-elemental composition of Eros has been measured independently by XRS (*Trombka et al.,* 2000) and by GRS (*Evans et al.,* 2001). The XRS data from orbit are consistent with an ordinary chondritic composition. The XRS did not find any evidence for spatial heterogeneity in composition. The XRS-measured element ratios Fe/Si, Al/Si, and Mg/Si were consistent with chondritic values, but S/Si was depleted from chondritic values. The XRS is sensitive to element ratios only within the uppermost few tens of microns depth, and it is not clear whether the S depletion is a surface effect due to impact devolatilization or a bulk Eros phenomenon that suggests removal of partial melt at the time Eros was part of its parent body.

The GRS observations had lower signal levels than predicted, and the highest-precision elemental abundance ratios were measured from the landing site on the southeast border of Himeros (*Evans et al.,* 2001), with the instrument at rest within a meter of the surface. Significantly, the landing site is within a pond. The GRS surface data showed the Mg/Si and Si/O ratios and the abundance of K to be consistent with chondritic values, but found Fe/Si and Fe/O to be lower than chondritic. The GRS data are sensitive to a depth of tens of centimeters, so this measurement pertains specifically to a volume on the order of a cubic meter of Eros. It is unclear from the GRS data whether the depletion of Fe results from partial melting or from sorting of the particles in the pond that removed lower-Fe silicates from Fe-Ni metal. Clear evidence from MSI images for depletion of large particles in ponds (*Robinson et al.,* 2001; *Veverka et al.,* 2001a) and the lack of evidence for Fe depletion in XRS data covering more representative areas of the surface support the latter interpretation. However, these analyses are preliminary and their implications are unclear.

The silicate mineralogy of Eros was inferred from visible and NIR spectra to be consistent with ordinary chondrites, using measurements of the 1-μm mafic absorption band center vs. the band area ratio [2-μm pyroxene absorption band area/1-μm mafic band area (*Gaffey et al.,* 1993b)] obtained by NIS and MSI (*Bell et al.,* 2002). The visible and NIR spectra are inconsistent with known primitive achondrites (*Burbine et al.,* 2001). Eros has neither melted nor differentiated fully, but some degree of partial melting or differentiation is possible. The spatially resolved measurements revealed no convincing evidence for compositional variation.

There is no evidence for intrinsic magnetization of Eros (*Acuña et al.,* 2000). No evidence of magnetization at Eros was observed even during the descent to the surface. The absence of magnetization may be consistent with a thermal history in which Eros was never heated to melting.

10. CONCLUSION AND FUTURE PROSPECTS

NEAR substantially increased our knowledge of primitive bodies in the solar system by providing a long, closeup look at the S-type asteroid 433 Eros and the first resolved images of the C-type asteroid 253 Mathilde. *NEAR* was the first mission to a near-Earth asteroid and a C-type asteroid, and it was the first spacecraft to flyby, orbit, and land on a small body. We have learned much from *NEAR,* but much remains to be learned.

At Mathilde, the *NEAR* flyby imaged only one face of the asteroid. The volume and density could only be estimated, but for any plausible volume, the density of Mathilde would be low enough to imply a high porosity. *NEAR* did not obtain any new information on the rotation state or the cause of the slow rotation, nor did it obtain any spatially

resolved spectral data. Nevertheless, the *NEAR* flyby of Mathilde provided important confirmation of the existence of large, highly porous main-belt asteroids. *NEAR*'s brief glimpse of Mathilde left us with fascinating questions: Is its composition related to that of carbonaceous chondrites? What is the nature of the porosity? To what extent did internal structures survive within Mathilde?

NEAR gathered much more detailed information at Eros. The low-order gravity harmonics as inferred from the spacecraft orbit agreed well with those inferred from the shape, assuming a constant density (*Yeomans et al.,* 2000), indicating that only small density variations can be present. Initial analyses suggested a small offset of the center of figure from the center of mass, consistent with a lower-density regolith layer up to 100 m thick (*Zuber et al.,* 2000). Further work is needed to assess the significance of this offset.

Images and laser altimetry from *NEAR Shoemaker* have provided strong evidence that Eros has a regolith cover and a consolidated but fractured substrate. Although angles of repose on Eros fall in the expected range for an unconsolidated regolith (*Zuber et al.,* 2000; *Cheng et al.,* 2002), the cohesive strength of bulk Eros is not usefully constrained by *NEAR* observations. The observations of jointed craters and structurally controlled craters imply the presence of a substrate with cohesive strength exceeding the gravitational stress, but the latter is very small on Eros. Even a cohesion of 0.1 MPa, which is easily exceeded by terrestrial clays, would be comparable to ~100 m overburden on Eros. The "consolidated substrate" of Eros may be weak enough to crumble easily in one's hand, or it may be much stronger. The geometric relations of grooves on Eros are in some cases suggestive of fractures in competent rock. The degree to which the interior has been fractured, and the nature of the porosity, also bear upon the efficiency with which seismic energy is transmitted across Eros. This efficiency may depend on the wave amplitude, so that weak seismic waves are transmitted with little damping, whereas stronger waves, which impose stresses sufficient to cause failure or to collapse pore space, may be highly damped.

High-resolution imaging — down to a few centimeters per pixel — revealed a complex and active regolith, with many puzzling features (*Veverka et al.,* 2001a). Why are there so few craters on Eros at small sizes under 100-m diameter, and why are there so many blocks at tens of meters and below? Why does the regolith appear to be more than 100 m deep in some regions, but much less in others? What makes ponds and debris aprons around some large blocks? What produces the albedo contrasts on Eros, which are much greater than on Ida or Gaspra (see, for example, Fig. 10)?

NEAR obtained its principal, spatially resolved NIR dataset from the initial low-phase flyby of Eros on February 14, 2000 (*Bell et al.,* 2002). The NIR spectra were consistent with an ordinary chondrite composition, but did not establish a link to a specific meteorite type. Moreover, why are spectral properties so homogeneous over the observed region in the northern hemisphere? Is the mineral composition in the optically active surface layer itself so uniform?

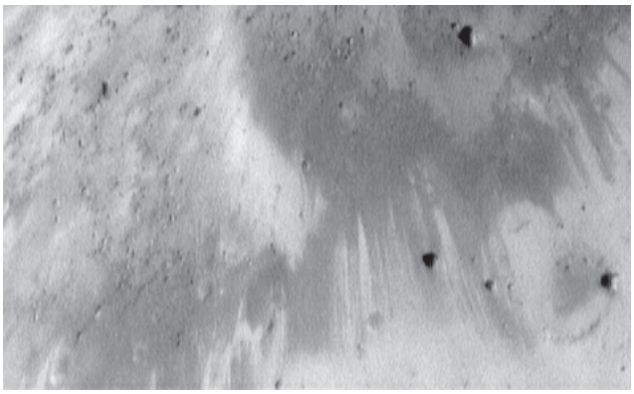

Fig. 10. Interior of crater Selene, diameter 3.6 km, showing albedo markings. Width of frame is 1.2 km. Streamers of dark material have slid downslope exposing lighter material. Many boulders can be seen (the Sun is to the right).

Even at the much-higher spatial resolutions achieved by the MSI, color variations were extremely subtle, and notably so in comparison with *Galileo* images of Ida and Gaspra (*Veverka et al.,* 2000). On Ida, relatively blue units (with a stronger 1-μm band) could be identified with fresh craters and even associated with ejecta from crater Azzurra (*Geissler et al.,* 1996), but no such phenomena are found on Eros. Is the different orbital history of Eros perhaps responsible for the difference (*Chapman et al.,* 2002)? Eros is presently in a Mars-crossing (but not Earth-crossing) orbit, and numerical simulations suggest that it may evolve into an Earth-crossing orbit within 2 m.y. (*Michel et al.,* 1998). Eros formed in the main belt, where its orbit underwent slow, chaotic diffusion because of numerous weak resonances. When or how Eros evolved onto a planet-crossing orbit cannot now be reconstructed with assurance, although the impact rate on Eros declined drastically once its orbit departed from the main belt (*Michel et al.,* 1998). Does such a cratering history explain the appearance of Eros, with its saturation density of craters >200 m, much lower densities of smaller craters, and extremely homogeneous color properties (*Chapman et al.,* 2002)?

The *NEAR* XRS/GRS experiment, even in its low-altitude orbits, observed both X-ray and γ-ray signal levels that were lower than predicted prelaunch. The X-ray and γ-spectra were puzzling (*McCoy et al.,* 2002; *Nittler et al.,* 2002; *Evans et al.,* 2001) and did not establish a definite meteorite link. Is Eros actually unrelated to any known meteorite type, or is it actually chondritic at depth, below the surface layers that may have been altered and fractionated by unknown weathering processes?

Finally, the lack of magnetization of Eros is a most surprising result. Why are most meteorites — including chondrites — much more strongly magnetized than Eros?

Much more work remains to be done with the wealth of data returned by *NEAR,* but many of the outstanding questions may be resolved only by another mission to Eros, one that might land on the surface, make *in situ* measurements

TABLE 4. Proposed Eros nomenclature.

Number	Name	Latitude	Longitude	Radius* (km)	Diameter (km)	Image
1	Himeros	21.16	282.32	4.99	~10	129267230
2	Psyche	31.60	94.61	3.29	4.85	128771856
3	Jahan	74.16	293.46	5.68	2.06	131586807
4	Mahal	79.36	169.98	5.38	1.16	131586807
5	Zhara	67.14	185.59	5.92	1.03	131585647
6	Fortunio	63.09	221.27	6.40	1.15	131575647
7	Viviane	46.58	236.01	6.85	0.94	131551436
8	Tutanekai	56.36	3.33	6.53	2.10	130420057
9	Narcissus	18.15	7.12	12.60	2.91	131232807
10	Leander	25.61	210.34	9.40	1.39	131530139
11	Valentine	14.64	208.43	10.53	2.21	132023740
12	Cupid	8.29	230.18	9.44	1.84	126711646
13	Don Juan	29.55	356.67	10.09	1.15	127388574
14	Avtandil	–22.53	233.10	8.36	1.16	135754887
15	Lolita	–35.17	197.67	8.58	1.81	137481063
16	Orpheus	25.56	176.74	11.37	1.07	135617746
17	Eurydice	13.49	170.03	13.52	2.24	132074943
18	Aida	7.94	130.50	4.93	1.66	129644551
19	Radames	–5.16	115.09	4.38	1.63	129644551
20	Genji	–19.50	88.62	4.37	1.52	129644551
21	Fujitsubo	–3.75	62.70	5.64	1.70	129644551
22	Hios	–9.41	130.90	4.98	1.26	129644551
23	Gamba	–20.58	54.13	6.41	1.27	129644551
24	Prosperina	–61.01	27.30	6.51	0.82	132640073
25	Selene	–14.18	12.53	13.48	3.64	131112223
26	Leylie	–3.01	23.48	15.87	1.88	131480043
27	Majnoon	3.76	28.80	15.52	2.06	131342359
28	Pao-yu	–73.20	105.58	5.49	0.84	134043704
29	Tai-yu	–47.02	126.06	4.81	1.40	131403667
30	Pygmalion	–1.85	191.09	15.33	1.75	128507342
31	Galatea	–10.17	183.05	15.23	1.38	131694511
32	Don Quixote	–57.70	250.82	6.23	0.88	135340688
33	Dulcinea	–76.13	272.86	6.05	1.40	137502634
34	Valentino	6.76	161.31	12.10	1.66	126723790
35	Abelard	–3.53	12.23	15.18	1.15	131112135
36	Heathcliff	7.35	167.89	15.42	1.09	131343205
37	Catherine	9.13	171.08	16.12	1.12	132207995

*Radius is distance from the Eros center, whereas diameter is the crater diameter.

such as seismic sounding, or perhaps even return samples. A more worthy, important, or fascinating target can hardly be imagined.

APPENDIX: EROS NOMENCLATURE

The Eros nomenclature system used in this chapter was proposed by the *NEAR Shoemaker* science team to the International Astronomical Union but had not been provisionally accepted as of November 2001. In this system, place names on Eros are names of famous lovers from literature, mythology, and history. Table 4 lists names of large craters on Eros. Two names of large features are not included in Table 4 although they have been used in publications. These are Shoemaker Regio [or simply Shoemaker crater (*Thomas et al.,* 2001)], and Rahe Dorsum, the 18-km ridge. Both features can be seen in Fig. 7.

Acknowledgments. I thank Scott Murchie and Peter Thomas for helpful comments. I also thank the many members of the *NEAR* team from the Applied Physics Laboratory, NASA Headquarters, NASA centers, universities, and industry for their hard work and dedication. This work was supported by NASA.

REFERENCES

Acuña M., Russell C., Zanetti L., and Anderson B. (1997) Magnetic field investigation: Science objectives at asteroid 433 Eros and experimental approach. *J. Geophys. Res., 102,* 23751–23759.

Acuña M. H., Anderson B. J., Russell C. T., Wasilewski P., Kletetshka G., Zanetti L., and Omidi N. (2002) NEAR magnetic field observations at 433 Eros: First measurements from the surface of an asteroid. *Icarus,* in press.

Barnouin-Jha O. S., Garvin J. B., Cheng A. F., Zuber M., Smith D., Neumann G., Murchie S., Robinson M., and Veverka J. (2001) Preliminary impact crater dimensions on 433 Eros from the NEAR laser range-finder and imager (abstract). In *Lunar and Planetary Science XXXII,* Abstract #1786. Lunar and Planetary Institute, Houston (CD-ROM).

Bell J., Davis D., Hartmann W., and Gaffey M. (1989) Asteroids: The big picture. In *Asteroids II* (R. P. Binzel et al., eds.), pp. 921–945. Univ. of Arizona, Tucson.

Bell J. F. III, Izenberg N. I., Lucey P. G., Clark B. E., Peterson C., Gaffey M. J., Joseph J., Carcich B., Harch A., Bell M. E., Warren J., Martin P. D., McFadden L. A., Wellnitz D., Murchie S., Winter M., Veverka J., Thomas P., Robinson M. S., Malin M., and Cheng A. (2002) Near-IR reflectance spectroscopy of 433 Eros from the NIS instrument on the NEAR mission: 1. Low phase angle observations. *Icarus, 155,* 119–144.

Belton M. J. S., Veverka J., Thomas P., Helfenstein P., Simonelli D., Chapman C., Davies M. E., Greeley R., Greenberg R., Head J., Murchie S., Klaasen K., Johnson T. V., McEwen A., Morrison D., Neukum G., Fanale F., Anger C., Carr M., and Pilcher C. (1992) Galileo encounter with 951 Gaspra: First pictures of an asteroid. *Science, 257,* 1647–1652.

Belton M. J. S., Chapman C. R., Veverka J., Klaasen K. P., Harch A., Greeley R., Greenberg R., Head J. W. III, McEwen A., Morrison D., Thomas P. C., Davies M. E., Carr M. H., Neukum G., Fanale F. P., Davis D. R., Anger C., Gierasch P. J., Ingersoll A. P., and Pilcher C. B. (1994) First images of 243 Ida. *Science, 265,* 1543–1547.

Belton M. J. S., Mueller B. E. A., D'Amario L. A., Byrnes D. V., Klaasen K. P., Synnott S., Breneman H., Johnson T. V., Thomas P. C., Veverka J., Harch A. P., Davies M. E., Merline W. J., Chapman C. R., Davis D., Denk T., Neukum G., Petit J.-M., Greenberg R., Storrs A., and Zellner B. (1996) The discovery and orbit of 1993 (243)1 Dactyl. *Icarus, 120,* 185–199.

Binzel R. P. and Xu S. (1993) Chips off of asteroid 4 Vesta: Evidence for the parent body of basaltic achondrites. *Science, 260,* 186–191.

Binzel R. P., Burbine T. H., and Bus S. J. (1996) Groundbased reconnaissance of asteroid 253 Mathilde: Visible wavelength spectrum and meteorite comparison. *Icarus, 119,* 447–449.

Bottke W. F., Rubincam D., and Burns J. (2000) Dynamical evolution of main belt asteroids: Numerical simulations incorporating planetary perturbations and Yarkovsky thermal forces. *Icarus, 145,* 301–331.

Burbine T. H., McCoy T. J., Nittler L. R., and Bell J. F. III (2001) Could 433 Eros have a primitive achondritic composition? (abstract). In *Lunar and Planetary Science XXXII,* Abstract #1860. Lunar and Planetary Institute, Houston (CD-ROM).

Chapman C. R. (1996) S-type asteroids, ordinary chondrites, and space weathering: The evidence from Galileo's fly-bys of Gaspra and Ida. *Meteoritics & Planet. Sci., 31,* 699–725.

Chapman C. R., Merline W. J., and Thomas P. (1999) Cratering on Mathilde. *Icarus, 140,* 28–33.

Chapman C. R., Merline W. J., Thomas P. C., Joseph J., Cheng A. F., and Izenberg N. (2002) Impact history of Eros: Craters and boulders. *Icarus, 155,* 104–118.

Cheng A. F. and Barnouin-Jha O. (1999) Giant craters on Mathilde. *Icarus, 140,* 34–48.

Cheng A. F., Santo A., Heeres K., Landshof J., Farquhar F., Gold R., and Lee S. (1997) Near Earth Asteroid Rendezvous: Mission overview. *J. Geophys. Res., 102,* 23695–23708.

Cheng A. F., Cole T., Zuber M., Smith D. E., Guo Y., and Davidson F. (2000) In-flight calibration of the Near Earth Asteroid Rendezvous laser rangefinder. *Icarus, 148,* 572–586.

Cheng A. F., Barnouin-Jha O., Zuber M., Veverka J., Smith D. E., Neumann G., Robinson M., Thomas P., Garvin J., Murchie S., Chapman C., and Prockter L. (2001) Laser altimetry of small-scale features on 433 Eros from NEAR Shoemaker. *Science, 292,* 488–491.

Cheng A. F., Barnouin-Jha O., Prockter L., Zuber M., Neumann G., Smith D. E., Garvin J., Robinson M., Veverka J., and Thomas P. (2002) Small scale topography of 433 Eros from laser altimetry and imaging. *Icarus, 155,* 51–74.

Clark B. E., Veverka J., Helfenstein P., Thomas P. C., Bell J. F. III, Harch A., Robinson M. S., Murchie S. L., McFadden L. A., and Chapman C. R. (1999) NEAR photometry of asteroid 253 Mathilde. *Icarus, 140,* 53–65.

Clark B. E., Lucey P. G., Helfenstein P., Bell J. F. III, Peterson C., Veverka J., McConnochie T., Robinson M. S., Bussey B., Murchie S., Izenberg N., and Chapman C. (2001) Space weathering on Eros: Constraints from albedo and spectral measurements of Psyche Crater. *Meteoritics & Planet. Sci., 36,* 1617–1637.

Cole T. D., Boies M. T., El-Dinary A. S., Cheng A., Zuber M. T., and Smith D. E. (1997) The Near-Earth Asteroid Rendezvous laser altimeter. *Space Sci. Rev., 82,* 217–254.

Davis D. (1999) The collisional history of asteroid 253 Mathilde. *Icarus, 140,* 49–52.

Davis D. R., Ryan E., and Farinella P. (1994) Asteroid collisional evolution: Results from current scaling algorithms. *Planet. Space Sci., 42,* 599–610.

Evans L., Starr R., Trombka J., McClanahan T., Bailey S., Mikheeva I., Bhangoo J., Brueckner J., and Goldsten J. (2000) *Icarus, 148,* 95–117.

Evans L., Starr R., Brückner J., Reedy R., Boynton W., Trombka J., Goldsten J., Masarik J., Nittler L., and McCoy T. (2001) Elemental composition from gamma-ray spectroscopy of the NEAR-Shoemaker landing site on 433 Eros. *Meteoritics & Planet. Sci,* in press.

Gaffey M. J., Burbine T. H., and Binzel R. P. (1993a) Asteroid spectroscopy: Progress and perspectives. *Meteoritics, 28,* 161–187.

Gaffey M. J., Bell J. F., Brown R. H., Burbine T. H., Piatek J. L., Reed K. L., and Chaky D. A. (1993b) Mineralogical variations within the S-type asteroid class. *Icarus, 106,* 573–602.

Geissler P., Petit J-M., Durda D. D., Greenberg R., Bottke W., Nolan M., and Moore J. (1996) Erosion and ejecta reaccretion on 243 Ida and its moon. *Icarus, 120,* 140–157.

Goldsten J. O., McNutt R. L. Jr., Gold R. E., Gary S. A., Fiore E., Schneider S. E., Hayes J. R., Trombka J. I., Floyd S. R., Boynton W. V., Bailey S., Brückner J., Squyres S. W., Evans L. G., Clark P. E., and Starr R. (1997) The X-ray/gamma-ray spectrometer on the Near Earth Asteroid Rendezvous mission. *Space Sci. Rev., 82,* 169–216.

Greenberg R., Bottke W., Nolan M., Geissler P., Petit J.-M., and Durda D. (1996) Collisional and dynamical history of Ida. *Icarus, 120,* 106–118.

Harris A. (1994) Tumbling asteroids. *Icarus, 107,* 209–211.

Hawkins S. E. III, Darlington E. H., Murchie S. L., Peacock K., Harris T. J., Hersman C. B., Elko M. J., Prendergast D. T.,

Ballard B. W., Gold R. E., Veverka J., and Robinson M. S. (1997) Multi-spectral imager on the Near Earth Asteroid Rendezvous mission. *Space Sci. Rev., 82,* 31–100.

Heeres K. J., Holland D., and Cheng A. F. (1997) The NEAR science data center. *Space Sci. Rev., 82,* 283–308.

Housen K. R., Holsapple K. A., and Voss M. E. (1999) Compaction as the origin of the unusual craters on the asteroid Mathilde. *Nature, 402,* 155–157.

Izenberg N. and Anderson B. (1998) NEAR swings by Earth en route to Eros. *Eos Trans. AGU, 79,* 289, 294–295.

Izenberg N. I., Bell J. F. III, Warren J. W., Martin P., Peacock K., Darlington E. H., Heyler G., Murchie S. L., McFadden L., Wellnitz D., Clark B., Joseph J., Carcich B., Harch A., Robinson M., Chapman C., Merline B., and Veverka J. (2000) Inflight calibration of the Near Earth Asteroid Rendezvous mission's Near Infrared Spectrometer I. Initial calibrations. *Icarus, 148,* 550–571.

Kivelson M., Bargatze L., Khurana K., Southwood D., Walker R., and Coleman P. (1993) Magnetic field signatures near Galileo's closest approach to Gaspra. *Science, 261,* 331–334.

Landshof J. and Cheng A. F. (1995) NEAR mission and science operations. *J. Astronaut. Sci., 43,* 477–489.

Lohr D. A., Zanetti L. J., Anderson B. J., Potemra T. A., Hayes J. R., Gold R. E., Henshaw R. M., Mobley F. F., Holland D. B., Acuña M. H., and Scheifele J. L. (1997) NEAR magnetic field investigation, instrumentation, spacecraft magnetics and data access. *Space Sci. Rev., 82,* 255–281.

McCord T., Adams J., and Johnson T. V. (1970) Asteroid Vesta: Spectral reflectivity and compositional implications. *Science, 168,* 1445–1447.

McCoy T. J. et al. (2002) The composition of 433 Eros: A mineralogical-chemical synthesis. *Meteoritics & Planet. Sci., 36,* 1661–1672.

Melosh H. and Ryan E. (1997) Asteroids: Shattered but not dispersed. *Icarus, 129,* 562–564.

Michel P., Farinella P., and Froeschle C. (1998) Dynamics of Eros. *Astron J., 116,* 2023–2031.

Mottola S. W., Sears D., Erikson A., Harris A. W., Young J. W., Hahn G., Dahlgren M., Mueller B. E. A., Owen B., Gil-Hutton R., Licandro J., Barrucci M. A., Angeli C., Neukum G., Lagerkvist C. I., and Lahulla J. F. (1995) The slow rotation of 253 Mathilde. *Planet. Space Sci., 43,* 1609–1613.

Murchie S. and Pieters C. (1996) Spectral properties and rotational spectral heterogeneity of 433 Eros. *J. Geophys. Res., 101,* 2201–2214.

Murchie S., Robinson M., Hawkins S. E. III, Harch A., Helfenstein P., Thomas P., Peacock K., Owen W., Heyler G., Murphy P., Darlington E. H., Keeney A., Gold R., Clark B., Izenberg N., Bell J. F. III, Merline W., and Veverka J. (1999) Inflight calibration of the NEAR multispectral imager. *Icarus, 140,* 66–91.

Murchie S., Domingue D., Robinson M., Li H., Prockter L., Hawkins S. E., Owen W., and Clark B. (2002a) Inflight calibration of the NEAR multispectral imager: 2. Results at Eros. *Icarus, 155,* 229–243.

Murchie S., Robinson M., Clark B., Li H., Thomas P., Joseph J., Bussey B., Domingue D., Veverka J., Izenberg N., and Chapman C. (2002b) Color variations on Eros from NEAR multispectral imaging. *Icarus, 155,* 145–168.

NEAR Science Working Group (1986) *Near Earth Asteroid Rendezvous.* JPL Report 86-7.

Nittler L. R. et al. (2002) X-ray fluorescence measurements of the surface elemental composition of asteroid 433 Eros. *Meteoritics & Planet. Sci., 36,* 1673–1696.

Ostro S., Pravec P., Benner L., Hudson S., Šarounová L., Hicks M., Rabinowitz D., Scotti J., Tholen D., Wolf W., Jurgens R., Thomas M., Giorgini J., Chodas P., Yeomans D., Rose R., Frye R., Rosema K., Winkler R., and Slade M. (1999) Radar and optical observations of asteroid 1998 KY26. *Science, 285,* 557–559.

Pravec P. and Harris A. W. (2001) Asteroid rotations. Presentation at the Asteroids 2001 conference.

Prockter L., Thomas P., Robinson M., Joseph J., Milne A., Bussey B., Veverka J., and Cheng A. (2002) Surface expressions of structural features on Eros. *Icarus, 155,* 75–93.

Rivkin A., Clark B., Britt D., and Lebofsky L. (1997) Infrared spectrophotometry of the NEAR flyby target 253 Mathilde. *Icarus, 127,* 255–257.

Robinson M. S., Thomas P. C., Veverka J., Murchie S., and Carcich B. T. (2001) Morphology, distribution and origin of ponded deposits on Eros. *Nature, 413,* 396–400.

Santo A., Lee S., and Gold R. (1995) NEAR spacecraft and instrumentation. *J. Astronaut. Sci., 43,* 373–398.

Starr R., Clark P., Murphy M., Floyd S., McClanahan T., Nittler L., Trombka J., Evans L., Boynton W., Bailey S., Bhangoo J., Mikheeva I., Brueckner J., Squyres S., McCartney E., Goldsten J., and McNutt R. (2000) Instrument calibrations and data analysis procedures for the NEAR x-ray spectrometer. *Icarus, 147,* 498–519.

Thomas P. C., Veverka J., Simonelli D., Helfenstein P., Carcich B., Belton M. J. S., Davies M. E., and Chapman C. (1994) The shape of Gaspra. *Icarus, 107,* 23–36.

Thomas P. C., Veverka J., Bell J. F. III, Clark B. E., Carcich B., Joseph J., Robinson M., McFadden L. A., Malin M. C., Chapman C. R., Merline W., and Murchie S. (1999) Mathilde: Size, shape, and geology. *Icarus, 140,* 17–27.

Thomas P. C., Robinson M. S., Veverka J., and Murchie S. (2001) Shoemaker crater as a major source of ejecta on asteroid 433 Eros. *Nature, 413,* 394–396.

Thomas P. C., Joseph J., Carcich B., Veverka J., Clark B. E., Bell J. F. III, Byrd A. J., Chomko R., Robinson M., Murchie S., Prockter L., Cheng A., Izenberg N., Malin M., Chapman C., McFadden L. A., Kirk R., Gaffey M., and Lucey P. G. (2002) Eros: Shape, topography, and slope processes. *Icarus, 155,* 18–37.

Trombka J., Floyd S., Boynton W., Bailey S., Brueckner J., Squyres S., Evans L., Clark P., Starr R., Fiore E., Gold R., Goldsten J., and McNutt R. (1997) Compositional mapping with the NEAR x-ray/gamma ray spectrometer. *J. Geophys. Res., 102,* 23729–23750.

Trombka J., Squyres S., Brückner J., Boynton W., Reedy R., McCoy T., Gorenstein P., Evans L., Arnold J., Starr R., Nittler L., Murphy M., Mikheeva I., McNutt R., McClanahan T., McCartney E., Goldsten J., Gold R., Floyd S., Clark P., Burbine T., Bhangoo J., Bailey S., and Petaev M. (2000) The elemental composition of asteroid 433 Eros: Results of the NEAR-Shoemaker x-ray spectrometer. *Science, 289,* 2101–2105.

Veverka J., Bell J. F., Thomas P., Harch A., Murchie S., Hawkins S., Warren J., Darlington E., Peacock K., Chapman C., McFadden L., Malin M., and Robinson M. (1997a) An overview of the NEAR multispectral imager-near infrared spectrometer investigation. *J. Geophys. Res., 102,* 23709–23727.

Veverka J., Thomas P., Harch, A., Clark B., Bell J. F. III, Carcich B., Joseph J., Chapman C., Merline W., Robinson M., Malin

M., McFadden L. A., Murchie S., Hawkins S. E. III, Farquhar R., Izenberg N., and Cheng A. (1997b) NEAR's flyby of 253 Mathilde: Images of a C asteroid. *Science, 278,* 2109–2114.

Veverka J. et al. (1999a) Imaging of asteroid 433 Eros during NEAR's flyby reconnaissance. *Science, 285,* 562–564.

Veverka J., Thomas P., Harch A., Clark B., Bell J. F. III, Carcich B., Joseph J., Murchie S., Izenberg N., Chapman C., Merline W., Malin M., McFadden L., and Robinson M. (1999b) NEAR encounter with asteroid 253 Mathilde: Overview. *Icarus, 140,* 3–16.

Veverka J., Robinson M., Thomas P., Murchie S., Bell J. F. III, Izenberg N., Chapman C., Harch A., Bell M., Carcich B., Cheng A., Clark B., Domingue D., Dunham D., Farquhar R., Gaffey M. J., Hawkins E., Joseph J., Kirk R., Li H., Lucey P., Malin M., Martin P., McFadden L., Merline W. J., Miller J. K., Owen W. M. Jr., Peterson C., Prockter L., Warren J., Wellnitz D., Williams B. G., and Yeomans D. K. (2000) NEAR at Eros: Imaging and spectral results. *Science, 289,* 2088–2097.

Veverka J., Thomas P. C., Robinson M., Murchie S., Chapman C., Bell M., Harch A., Merline W. J., Bell J. F. III, Busey B., Carcich B., Cheng A., Clark B., Domingue D., Dunham D., Farquhar R., Gaffey M. J., Hawkins E., Izenberg N., Joseph J., Kirk R., Li H., Lucey P., Malin M., McFadden L., Miller J. K., Owen W. M. Jr., Peterson C., Prockter L., Warren J., Wellnitz D., Williams B. G., and Yeomans D. K. (2001a) Imaging of small-scale features on 433 Eros from NEAR: Evidence for a complex regolith. *Science, 292,* 484–488.

Veverka J., Farquhar B., Robinson M., Thomas P., Murchie S., Harch A., Antreasian P. G., Chesley S. R., Miller J. K., Owen W. M. Jr., Williams B. G., Yeomans D., Dunham D., Heyler G., Holdridge M., Nelson R. L., Whittenburg K. E., Ray J. C., Carcich B., Cheng A., Chapman C., Bell J. F. III, Bell M., Bussey B., Clark B., Domingue D., Gaffey M. J., Hawkins E., Izenberg N., Joseph J., Kirk R., Lucey P., Malin M., McFadden L., Merline W. J., Peterson C., Prockter L., Warren J., and Wellnitz D. (2001b) The landing of the NEAR-Shoemaker spacecraft on asteroid 433 Eros. *Nature, 413,* 390–393.

Warren J. W., Peacock K., Darlington E. H., Murchie S. L., Oden S. F., Hayes J. R., Bell J. F. III, Krein S. J., and Mastandrea A. (1997) Near infrared spectrometer for the Near Earth Asteroid Rendezvous mission. *Space Sci. Rev., 82,* 101–167.

Wilkison S. L., Robinson M. S., Thomas P. C., Veverka J., McCoy T. J., Murchie S. L., Prockter L., and Yeomans D. (2001) An estimate of Eros's porosity and implications for internal structure. *Icarus,* in press.

Xu S., Binzel R., Burbine T., and Bus S. (1995) Small main belt asteroid spectroscopic survey: Initial results. *Icarus, 115,* 1–35.

Yeomans D. (1995) Asteroid 433 Eros: The target body of the NEAR mission. *J. Astronaut. Sci., 43,* 417–426.

Yeomans D., Konopliv A., and Barriot J. (1997a) NEAR radio science investigations. *J. Geophys. Res., 102,* 23775–23780.

Yeomans D. et al. (1997b) Estimating the mass of asteroid 253 Mathilde from tracking data during the NEAR flyby. *Science, 278,* 2106–2109.

Yeomans D. K., Antreasian P. G., Cheng A., Dunham D. W., Farquhar R. W., Gaskell R. W., Giorgini J. D., Helfrich C. E., Konopliv A. S., McAdams J. V., Miller J. K., Owen W. M. Jr., Thomas P. C., Veverka J., and Williams B. G. (1999) Estimating the mass of asteroid 433 Eros during the NEAR spacecraft flyby. *Science, 285,* 560–562.

Yeomans D. K., Antreasian P. G., Barriot J.-P., Chesley S. R., Dunham D. W., Farquhar R. W., Giorgini J. D., Helfrich C. E., Konopliv A. S., McAdams J. V., Miller J. K., Owen W. M. Jr., Scheeres D. J., Thomas P. C., Veverka J., and Williams B. G. (2000) Radio science results during the NEAR-Shoemaker spacecraft rendezvous with Eros. *Science, 289,* 2085–2088.

Zuber M. T., Smith D. E., Cheng A. F., and Cole T. D. (1997) The NEAR laser ranging investigation. *J. Geophys. Res., 102,* 23761–23773.

Zuber M. T., Smith D. E., Cheng A. F., Garvin J. B., Aharonson O., Cole T. D., Dunn P. J., Guo Y., Lemoine F. G., Neumann G. A., Rowlands D. D., and Torrence M. H. (2000) The shape of 433 Eros from the NEAR-Shoemaker Laser Rangefinder. *Science, 289,* 2097–2101.